Machinery & Energetics
Vol. 16, No. 4. 2025

Journal homepage:
https://technicalscience.com.ua/en

UDC 519.6:621.9.015:536.24
DOI: 10.31548/machinery/4.2025.53

Abdelhak Saoudi*
PhD Student
Laboratory of Engineering of Sciences of Advanced Materials – ISMA
Department of Mechanical Engineering, ABBES Laghrour University
40004, P.O. Box 1252, Batna Rd., Khenchela, Algeria
https://orcid.org/0000-0002-8295-1947

Belkacem Meddour
Professor
Laboratory of Engineering of Sciences of Advanced Materials – ISMA
Department of Mechanical Engineering, ABBES Laghrour University
40004, P.O. Box 1252, Batna Rd., Khenchela, Algeria
https://orcid.org/0000-0002-4751-2615

Badis Haddag
Associate Professor
LEM3 Laboratory, UMR CNRS 7239, Lorraine University
Institut Mines-Telecom (InSIC)
88100, 27 Voie de l'Innovation, Saint-Dié, France
https://orcid.org/0000-0003-3850-3044

Mohammed Salah Aggoune
PhD in Materials Engineering
Faculty of Science and Technology, Department of Mechanical Engineering
Echahid Cheikh Larbi Tebessi University
12000 Tebessa, Algeria
https://orcid.org/0000-0002-3385-7081

Abdelaziz Abboudi
Professor
Laboratory of Engineering of Sciences of Advanced Materials – ISMA
Department of Mechanical Engineering, ABBES Laghrour University
40004, P.O. Box 1252, Batna Rd., Khenchela, Algeria
https://orcid.org/0000-0002-1398-6070

Modelling and studying of thermal behaviour of thin layer using finite element method – application to coated tools

Abstract. The continuous evolution of thin-layer technologies is essential in modern dry machining, where effective thermal control of coated cutting tools is critical for limiting heat-induced wear and extending tool life. The purpose of this article was to investigate and model the thermal response of coated cutting tools and to evaluate the influence of single-layer and multilayer thin coatings on heat transfer during orthogonal dry cutting. To achieve this objective, a transient thermal model based on the finite element method was developed using a Galerkin formulation combined with an implicit Crank-Nicolson time integration scheme. The numerical framework was applied to three tool configurations: an uncoated WC-Co insert, a TiN-coated insert, and a TiN/Al_2O_3 double-coated insert. Experimental dry turning tests were conducted to validate the numerical predictions. The results showed that the numerical model accurately reproduced the temporal evolution of temperature at the tool-chip interface

Article's History: Received: 08.08.2025; Revised: 04.11.2025; Accepted: 27.11.2025.

Suggested Citation:
Saoudi, A., Meddour, B., Haddag, B., Aggoune, M.S., & Abboudi, A. (2025). Modelling and studying of thermal behaviour of thin layer using finite element method – application to coated tools. *Machinery & Energetics,* 16(4), 53-63. doi: 10.31548/machinery/4.2025.53.

*Corresponding author

and within the insert. The uncoated tool exhibited rapid heat penetration and pronounced internal thermal gradients. The TiN coating slightly increased the surface temperature but offered limited resistance to heat diffusion. In contrast, the TiN/Al_2O_3 multilayer configuration significantly restricted heat transfer towards the substrate, leading to lower internal temperatures and reduced thermal gradients. The Al_2O_3 layer acted as an effective thermal barrier, confining heat near the cutting edge and protecting the tool core from excessive thermal loading. These findings demonstrated that multilayer ceramic coatings provided superior thermal protection compared with single-layer coatings. The proposed finite element method approach could be effectively applied to coating design, tool optimisation, and thermal management in dry machining applications

Keywords: dry machining; heat transfer; numerical approach; cutting; temporal

INTRODUCTION

In industrial manufacturing, the optimisation of material systems and structural configurations is fundamental to ensuring reliability, service life, and overall process efficiency. Advances in thin-film engineering have enabled the deployment of high performance coatings designed to strengthen functional surfaces operating under severe thermomechanical loading. Within this context, hard protective coatings for cutting tools have become a critical element in modern machining. They increase productivity, extend tool life, and enable environmentally responsible dry or near dry cutting regimes. During metal cutting, extreme frictional contact and high interfacial temperatures develop at the tool chip interface, accelerating wear mechanisms and diminishing machining stability. To alleviate these effects, cutting inserts are commonly coated via physical vapour deposition (PVD) or chemical vapour deposition (CVD), two established techniques capable of forming dense, adherent, and mechanically robust layers engineered to resist thermal softening, oxidation, and mechanical abrasion. These coatings have been widely investigated, particularly within the broader framework of sustainable machining, where the control of heat generation and thermal gradients is essential for maintaining tool integrity under elevated cutting conditions.

Advances in modelling thin layer thermal behaviour have broadened numerical capabilities. A. Ifis *et al.* (2013) proposed the MAX-FEM (Matching Asymptotic eXtended Finite Element Method) approach, which eliminates the need for mesh refinement near thin interlayers by deriving correction matrices from matching asymptotic expansions (MAE) and integrating concepts from the Extended Finite Element Method (X-FEM). Implemented in Matlab, the model delivered significant reductions in computational cost relative to classical Finite Element Method (FEM) formulations. The Thermal Thin Shell Approximation (TSA), introduced by E. Schnaubelt *et al.* (2023), reformulates ultra-thin insulating layers into reduced order 2D surface elements while preserving accurate in plane and through-thickness heat flux descriptions. Validated across multiple configurations, including High-Temperature Superconducting (HTS) coils, TSA offers substantial reductions in degrees of freedom and computational overhead, making it particularly effective in systems where the insulation to conductor thickness ratio is extremely small.

Additional contributions reinforce the relevance of advanced thermal modelling in manufacturing. M. Ala *et al.* (2025) developed a 3D finite element thermal model to predict laser cladding bead geometry, integrating heat transfer, fluid flow, and melt pool dynamics within COMSOL. Validated by 18 experiments on Inconel 625, the model achieved errors below 13%, with results underscoring the critical role of Marangoni convection in melt pool morphology and additive manufacturing quality. D.H. Nguyen *et al.* (2008) extended the application of X-FEM by treating brazed joints as singularities within a matching asymptotic development (DAR) framework, enabling accurate resolution of both mechanical and transient thermal behaviours and achieving strong agreement with analytic and commercial FEM solutions.

G. Kumaran *et al.* (2021) highlighted the importance of multi physics models for analysing coupled thermal and mass transport phenomena in nanostructured coatings, reinforcing the strategic role of numerical simulation in surface engineering optimisation. Researchers I. Bencheikh *et al.* (2017) introduced a multiscale X-FEM/level-set methodology for coated cutting tools, achieving improved convergence characteristics and reduced computational cost in transient thermomechanical analyses, confirming the suitability of this framework for thin film coatings, brazed joints, and adhesively bonded interfaces. In a complementary study C Upadhyay *et al*. (2025) investigated the effect of TiAlN coating thickness (1-4 µm) during dry milling of AISI 1045. Their FEM simulations accurately predicted cutting forces, temperature rise, and crater wear progression, and experimental validation confirmed that a 3 µm TiAlN layer provided optimal thermomechanical performance through reduced force levels, attenuated peak temperatures, and enhanced surface finish.

Within this broader scientific landscape, FEM remains a powerful framework for analysing temperature fields in cutting tools because it accommodates multilayer coating architectures, complex contact interactions, and dynamic boundary conditions. The aim of the study was to analyse the temporal evolution and spatial distribution of temperature in coated and uncoated cutting inserts under dry orthogonal cutting conditions using the finite element method.

MATERIALS AND METHODS

Heat generation during machining mainly results from two mechanisms: severe plastic deformation of the workpiece material and intense friction at the tool chip interface. The heat produced was partially transferred to the cutting insert, where the temperature distribution depends heavily on the thermal conductivity of each layer of the coating system. In this analysis, the thermal conductivities adopted for the constituent materials were 59, 30, 7.5, and 25 $Wm^{-1}K^{-1}$, for WC-Co, TiCN, Al_2O_3, and TiN, respectively. Figure 1 illustrates the generic domain Ω and its boundaries Γ_1 and Γ_2, in accordance with the configuration used in previous research by F. Kone *et al.* (2011).

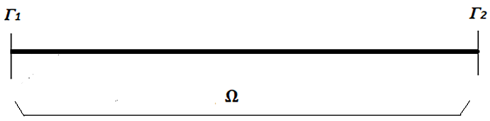

Figure 1. Domain and boundaries
Note: domain Ω and its boundaries Γ_1 and Γ_2
Source: developed by authors on the base on F. Kone *et al.* (2011)

In this general case, the transient heat conduction problem for the temperature field T(x ,t) was expressed in its strong form as follows:

$$\begin{cases} \rho c \frac{\partial T}{\partial t} - \operatorname{div}(\lambda \vec{\nabla} T) = \dot{\omega} \text{ in } \Omega \times]0,t[\\ T(x,0) = T_0 \ \forall x \in \Omega \\ \lambda \vec{\nabla} T . \vec{n} = \varphi_{imp} \text{ at } \Gamma_2 \times]0,t[\, , \end{cases} \quad (1)$$

where ρ – the mass density, c the specific heat capacity, – the internal heat generation, λ – the thermal conductivity, and φ_{imp} – the imposed heat flux density.

The corresponding weak formulation was written as follows:

$$\int_\Omega \rho c \frac{\partial T}{\partial t} \vartheta d\Omega + \int_\Omega \lambda \vec{\nabla} T . \vec{\nabla} \vartheta d\Omega = \int_\Omega \dot{\omega} \vartheta d\Omega + \int_{\Gamma_2} \varphi_{imp} \vartheta d\Gamma, \quad (2)$$

where, ϑ represented the test function.

To approximate the solution numerically, the domain Ω was discretised into Ne finite elements connected through Nn nodes. The temperature field was approximated using Equation (3):

$$T(x) = \sum_{i=1}^{N_n} N_i(x) T_i, \quad (3)$$

where $N_i(x)$ – the shape functions and T_i – the nodal temperatures.

Substituting (3) into the weak formulation (2) and removing the test functions yielded the classical finite element matrix representation:

$$[C]\left\{\frac{\partial T}{\partial t}\right\} + [K]\{T\} = \{Q\}, \quad (4)$$

where, {T} – the nodal temperature, [C] – the heat capacity matrix, [K] – the conductivity matrix, and {Q} – the thermal loading vector.

The components of these matrices and vectors were calculated as follows:

$$[K] = \sum_{e=1}^{N_e} \int_{\Omega_e} [B]^T [D][B] d\Omega \Leftrightarrow$$
$$\Leftrightarrow K_{ij} = \sum_{e=1}^{N_e} \int_{\Omega_e} \lambda \vec{\nabla} N_i \, \vec{\nabla} N_j d\Omega \, , \quad (5)$$

$$[C] = \sum_{e=1}^{N_e} \int_{\Omega_e} \rho c [N]^T [N] d\Omega \Leftrightarrow C_{ij} = \sum_{e=1}^{N_e} \int_{\Omega_e} \rho c N_i \, N_j d\Omega, \quad (6)$$

$$\{Q\} = \sum_{e=1}^{N_e} \left(\int_{\Omega_e} \dot{\omega} [N]^T d\Omega - \int_{\Gamma_e^2} \varphi_{imp} [N]^T d\Gamma \right) \Leftrightarrow$$
$$\Leftrightarrow Q_i = \sum_{e=1}^{N_e} \left(\dot{\omega} N_i d\Omega - \int_{\Gamma_e^2} \varphi_{imp} N_i d\Gamma \right). \quad (7)$$

For time integration, the Crank-Nicolson two step implicit scheme was adopted due to its stability and second order accuracy. Applying this method to (4) led to the recurrence relation:

$$\left(\frac{[C]}{\Delta t} + \frac{1}{2}[K]\right)\{T\}^{m+1} = \left(\frac{[C]}{\Delta t} + \frac{1}{2}[K]\right)\{T\}^m +$$
$$+ \frac{1}{2}\{Q\}^m + \frac{1}{2}\{Q\}^{m+1}, \quad (8)$$

which enabled computation of $\{T\}^{m+1}$ from the known "assumed" state $\{T\}^m$. The time step Δt had to satisfy the stability requirement (9) to ensure the stability of the resolution method:

$$\frac{1}{6} \leq \alpha \frac{\Delta t}{(\Delta x)^2} \leq \frac{1}{2}, \quad (9)$$

with α – the thermal diffusivity given by , and Δx – the mesh spacing in the region of highest thermal gradient.

The three cutting inserted configurations: uncoated WC-6%Co, single layer TiN, and double layer TiN+Al_2O_3 were modelled as 1D multilayer systems (Fig. 2). Each layer was discretised according to stability constraints associated with the Crank-Nicolson scheme. Table 1 summarises the mesh density for each configuration.

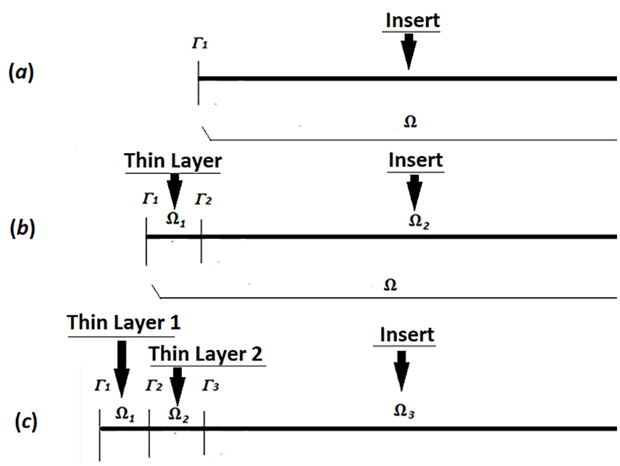

Figure 2. Domains, subdomains and boundaries
Note: a – uncoated carbide insert, b – coated carbide insert (TiN coating), c – double coated insert (coatings TiN+Al_2O_3)
Source: developed by authors

The machining conditions used to define the applied heat flux were derived from experimental measurements. In all simulations, the workpiece bottom surface moves at a cutting speed of 100 m/min, while the insert remains stationary. The undeformed chip thickness is maintained at 0.4 mm, with a clearance angle of 6°. The effective cutting length is 10 mm, corresponding to approximately 6 ms of machining time. A constant friction coefficient of 0.4 is adopted for all cases (Table 2).

Table 1. Meshing data

Case	Bodies	Number of elements
Uncoated	Insert	288
Coated insert	Coating	2
	Insert	397
Double coated insert	Coating 1	2
	Coating 2	2
	Insert	395

Note: number of elements
Source: developed by authors

Table 2. Cutting conditions

Parameter	Value
Cutting speed (m/min)	100
Undeformed chip thickness (mm)	0.4
Length of cut (mm)	10
Coefficient of friction	0.4
Cutting time (ms)	6

Note: cutting experimental conditions
Source: developed by authors

The local frictional heat flux in the contact zone was expressed as:

$$q_f = \tau s = \mu p s, \quad (10)$$

where μ – the local friction coefficient, τ – the shear stress, p – the contact pressure, and s – the sliding velocity. The resulting geometry, loading and boundary conditions of the cutting system were shown in Figure 3. Table 3 provides the thermal properties and dimensions for the substrate and coating layers employed in this study.

RESULTS AND DISCUSSION

As a first step in this study, it is important to verify the validity of the FEM numerical model that has been developed. To achieve this, the operating parameters were applied in the algorithm, and the resulting data were quantitatively compared with experimental measurements. For all analysed cases, the simulation begins at a temperature of 20°C, corresponding to the prescribed initial thermal condition $T = T_0 = 20°C$. The numerical evaluation of the tool surface temperature in the case of the uncoated insert (WC-Co) as presented in Figure 4, shows close agreement with the experimental measurements.

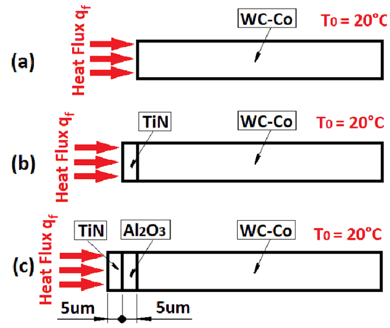

Figure 3. Geometry, dimensions, loading and boundary conditions of cutting tools and coating layers
Note: a – uncoated carbide insert, b – coated carbide insert (TiN coating), c – double coated insert (coatings $TiN + Al_2O_3$)
Source: developed by authors

Table 3. Thermal properties and dimensions

	Substrate	Coating	
	WC-Co	TiN	Al_2O_3
Conductivity ($W\ m^{-1}\ C^{-1}$)	59	25	7.5
ρCp ($Nmm^{-2}\ K^{-1}$)	15	12	3.42
Size (mm)	2	0.005	0.005

Note: thermal properties for numerical analysis
Source: developed by authors

Both curves show a rapid rise in temperature during the first 1 ms, reflecting intense heat generation on the cutting surface, followed by a slower increase. The experimental values slightly exceed the numerical predictions at most points, especially between 1 and 4 ms, where the maximum difference reaches about 50°C. After 4 ms, the curves converge towards a peak of about 456°C at 6 ms. In the case of the TiN coated insert (Fig. 5), the numerical evaluation of the tool surface temperature shows a comparable behavior to the experimental results, with a sharp rise during the first 1 ms due to the concentrated heat at the TiN layer, followed by a slower rise.

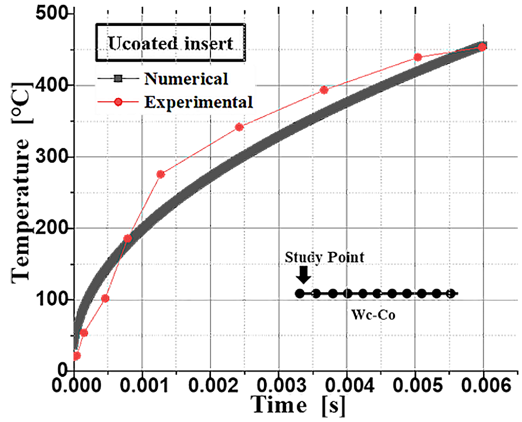

Figure 4. Temperature evolution at the tool surface of contact (Point study). Case of uncoated insert
Note: thermal properties (WC-Co) for numerical and cutting conditions for experimental
Source: developed by authors on the validation on research F. Kone *et al*. (2011)

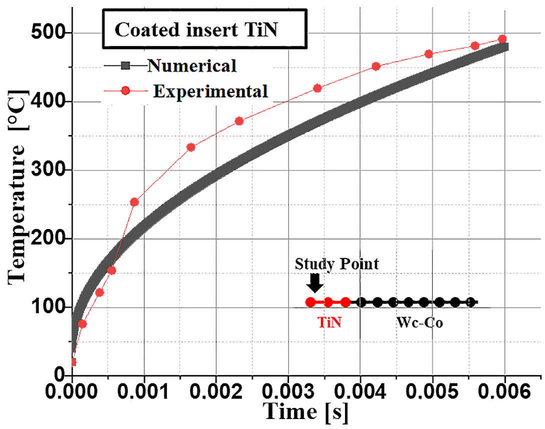

Figure 5. Temperature evolution at the tool surface of contact (Point study). Case of coated insert (TiN)
Note: thermal properties (WC-Co, TiN) for numerical and cutting conditions for experimental
Source: developed by authors on the validation on research F. Kone *et al.* (2011)

The experimental temperatures remain consistently higher than the numerical predictions, especially between 1 ms and 4 ms, where the maximum deviation is close to 60°C. After 4 ms, both curves gradually converge towards approximately 480°C at 6 ms. The double coated insert ($TiN+Al_2O_3$) as shows Figure 6 follows the numerical prediction of temperature evolution in the same general trend as the experimental results, with an initially sharp increase during the first 1 ms due to intense heat generation on the TiN layer. The experimental values remain higher than the numerical values, especially between 1 ms and 5 ms, where the maximum deviation reaches approximately 70°C, reflecting the added thermal resistance of the multilayer coat ($TiN+Al_2O_3$). After 5 ms, both curves gradually converge towards approximately 544°C at 6 ms. The slight temperature differences observed in all cases (Figs 4-6) tend to strengthen the credibility of the FEM model rather than weaken it. Real cutting tools, whether coated or uncoated, always have surface roughness, pores, and a heterogeneous grain structure, all of which increase friction and lead to local variations in heat generation. In contrast, our numerical model assumes a completely homogeneous material. Due to these natural industrial imperfections, it is to be expected that the experimental temperatures will be slightly higher. The fact that the FEM predictions are very close to the measurements despite these complexities proves that the model is accurate and reliable.

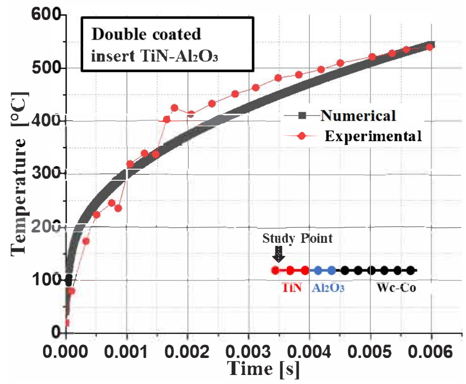

Figure 6. Temperature evolution at the tool surface of contact. Case of double coated insert ($TiN + Al_2O_3$)
Note: thermal properties (WC-Co, TiN and Al_2O_3) for numerical and cutting conditions for experimental
Source: developed by authors on the validation on research F. Kone *et al.* (2011)

With the finite element model's fidelity established, the model was extended to interrogate the internal thermal behaviour of the insert. Figures 7, 8 and 9 depict the simulated temperature evolution at critical nodes A, B, C, and D for each cutting condition, providing a quantitative analysis for interpreting temperature redistribution imposed by insert configuration rather uncoated, single layer coated, or double layer coated.

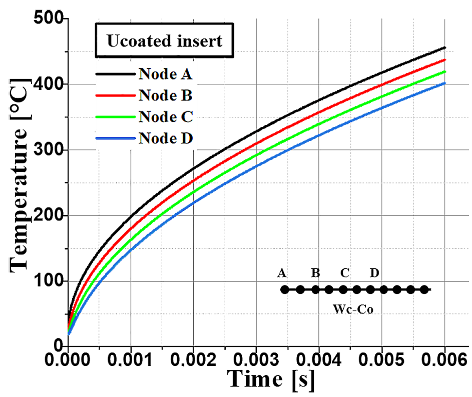

Figure 7. Temperature evolution at nodes. case of uncoated insert (WC-Co)
Note: node A: tool/chip interface, node B, node C and node D: WC-Co insert
Source: developed by authors

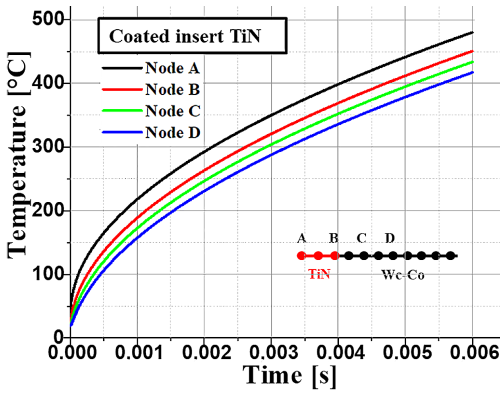

Figure 8. Temperature evolution at nodes. case of coated insert (TiN)

Note: node A: tool/chip interface, node B: TiN/WC-Co interface, node C and node D: WC-Co insert

Source: developed by authors

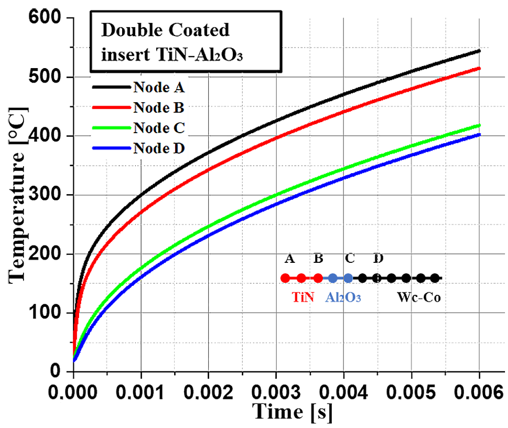

Figure 9. Temperature evolution at nodes. case of double coated insert ($TiN + Al_2O_3$)

Note: node A: tool/chip interface, node B: TiN/Al_2O_3 interface, node C: Al_2O_3/WC-Co interface, node D: WC-Co insert

Source: developed by authors

The numerical evaluation of the internal temperature distribution for the uncoated insert (WC-Co), shown in Figure 7, exhibits a clear thermal gradient along the nodes A to D. All four curves display a rapid temperature rise during the first 1 ms of cutting, reflecting the intense heat conducted directly into the WC-Co insert. Node A, being at the cutting edge (point of contact), reaches the highest temperature, followed in order by nodes B, C, and D, with a maximum difference of nearly 70°C between the extreme positions (A and D) at 6 ms. The temperature increase becomes progressively slower after the initial transient as the thermal field begin to stabilize, ultimately reaching about 456°C at node A. This behaviour confirms the absence of any thermal barrier, resulting in deep heat penetration and pronounced gradients inside the insert.

In the case of the TiN single layer coated insert (Fig. 8), the numerical prediction of temperature at the selected nodes shows a similar overall trend but with noticeably increased temperatures at all positions compered to Figure 7. As in the WC-Co uncoated case, node A exhibits the highest temperature, with a gradual decrease toward node D. The initial heat rises during the first 1 ms remains dominant due to the concentration of heat at the tool chip interface; however, the presence of the TiN layer results in higher heat transfer into the WC-Co insert, this can be seen by comparing temperature values of nodes B, C, and D in both Figures 7 and 8. By 6 ms, node A approaches roughly 480°C, while the deeper nodes remain significantly cooler.

For the double layer coated insert (Fig. 9), the predicted temperature evolution follows the same general trend as in the previous cases but with the lowest overall temperatures across the WC-Co insert. The presence of the $TiN + Al_2O_3$ double configuration introduces a stronger thermal resistance, resulting in an intensive and aggressive temperature rise at node A and B. During the first 1 ms, heat generation at the cutting edge (point of contact) still dominates, but the presence of the Al_2O_3 layer (from node B to node C) substantially restricts thermal diffusion into the underlying insert (WC-Co) which explain the 100°C temperature gap observed almost at all cutting duration. At 6 ms, node A reaches approximately 544°C, while the inner nodes (C and D) remain significantly cooler, with the smallest temperature spread among the three configurations (A and B, B and C, C and D). This confirms the enhanced insulating effect of the multilayer coating, which effectively limits internal heating and reduces thermal stresses within the tool.

The comparison between the three cases (Figs. 7-9) highlights the thermal management provided by the coatings. The uncoated WC-Co insert shows rapid heat transfer with a clear gradient ($\Delta T \approx 70$°C between nodes A and D) due to the absence of any barrier, resulting in deep internal heating. The single layer TiN coating does not mitigate this effect, but rather accelerates the process of heat transfer to the core of the WC-Co insert. In exchange, the double layer $TiN + Al_2O_3$ coating significantly enhances thermal resistance: While the cutting edge (nodes A and B) is still subjected to intense initial heating, the Al_2O_3 layer effectively limits heat diffusion to the inner nodes C and D, resulting in less heat diffusion and maintaining lower temperatures in the WC-Co insert. This demonstrates that the double coating not only enhances surface insulation, but also stabilizes the internal thermal distribution, reducing thermal stresses and protecting the core of the insert.

Plotting the temperature distribution profiles along the insert thickness reveals a very interesting thermal behaviour that clearly distinguishes between the three configurations (Fig. 10). The near surface region (0-0.1 mm) shows a very sharp gradient, confirming that heat remains highly concentrated at the interface between the tool and the chips. The uncoated insert shows the lowest surface temperature reaching about 450°C but has the smoothest gradient, indicating rapid heat transfer to the WC-Co core. The TiN single layer coating increases the surface temperature from 456°C to 480°C and makes the gradient steeper, indicating reduced thermal diffusion. The most pronounced effect is seen with the $TiN+Al_2O_3$ double coating, which produces the highest surface temperature of 544°C and the steepest gradient, confirming strong thermal insulation and minimal heat penetration outside the coated area. This characteristic is strongly interpreted by the low thermos conductivity and diffusivity of the Al_2O_3 layer, as shown in the by reference (Grzesik *et al.*, 2005). After about 0.1 mm, all curves converge, indicating that the multilayer system effectively protects the substrate by confining heat to the surface.

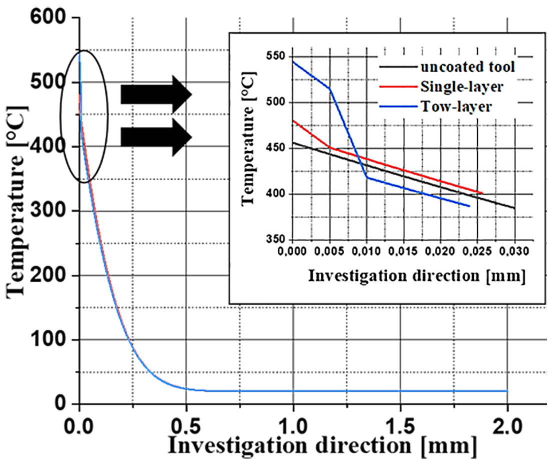

Figure 10. Detailing of temperature distribution inside the insert
Note: for all three cases t = 6 milliseconds
Source: developed by authors

The findings of this investigation, which utilised Finite Element Modelling (FEM) to analyse heat transfer and temperature evolution in coated tools during orthogonal dry cutting, are largely consistent with previous research on the thermal behaviour of coated tools. However, the results also reveal important distinctions that refine current understanding. The numerical simulations, validated by experimental measurements, offer a detailed depiction of temperature distribution at the tool chip interface and complement earlier analytical and numerical approaches reported in the literature. J. Zhang *et al.* (2022) demonstrated that the thermoconductivity and diffusivity of coating materials govern steady and transient temperature distributions, respectively, during cutting. The present study corroborates this finding by confirming the significant thermal barrier effect of Al_2O_3, whose low thermal conductivity markedly reduces heat penetration into the tool substrate. In contrast, TiN, as previously noted by J. Zhang *et al.*, provides limited thermal insulation. The current results refine this observation by quantifying the minimal thermal influence of TiN within an experimentally validated FEM framework, thereby offering stronger evidence for its limited role in thermal management during machining.

Similarly, the results of T.D. Ipilakyaa *et al.* (2024), who employed an equivalent layer methodology for multilayer coatings, emphasised the crucial role of coating thickness, layering sequence, and material thermal properties in the evolution of cutting temperature. Although the present study did not construct equivalent thermal layers but instead directly modelled physical coating architectures, both studies converge in showing that multilayer systems perform more effectively when a ceramic outer layer is used. The agreement further supports the suitability of analytical and numerical tools for predicting coating temperature, with the current FEM results achieving validated accuracy within the 10% error margin reported for their analytical models.

The numerical work of W. Grzesik *et al.* (2005) highlighted the ability of finite difference based simulations to capture coating-induced temperature field variations along the tool-chip interface, revealing strong dependencies on cutting speed and frictional conditions during orthogonal cutting. The present FEM investigation reaches comparable conclusions, showing that thermal contours strongly reflect coating composition and interface behaviour. However, by incorporating experimentally calibrated conditions and quantifying temperature evolution near the secondary shear zone with higher spatial resolution, this study extends the earlier numerical findings and provides a more comprehensive representation of heat transfer mechanisms occurring immediately upstream of the tool rake face, where direct measurement remains challenging. Previous studies by R. Komanduri & Z.B. Hou (2001) have shown that temperature fields within cutting tools and heat flux distributions along the rake face can be analysed using experimental measurements, analytical approaches, and numerical modelling. In numerical investigations by C.A. Van Luttervelt *et al.* (1998) and I. Lazoglu & Y. Altintas (2002), the heat transfer problem in metal cutting has been addressed using various computational methods, including the finite element method, the finite difference method, and the boundary element method, each with specific capabilities for resolving conductive, convective, and friction-induced heating phenomena. In the context of the present results, the finite element approach proved particularly effective for capturing the influence of coating architecture on thermal gradients and heat distribution near the tool-chip interface. Despite the extensive use of FEM in machining simulations, the present findings further highlight that the role of coating architecture, especially in the vicinity of the secondary shear zone, remains a critical factor governing internal heat transfer mechanisms and cannot be fully resolved without experimentally validated numerical models.

The contribution of tool coatings to mechanical stability has also been emphasised in previous research. P. Sahoo *et al.* (2020) demonstrated that coatings such as TiAlN enhance micro-milling stability by reducing tool wear and improving force modelling reliability. While the present study focused on temperature rather than force prediction or dynamic stability, the observed thermal benefits of Al_2O_3 coatings indirectly support the broader claims of stability enhancement. Lower temperatures are strongly associated with reduced wear and improved cutting performance, suggesting that the thermal barrier effect quantified in current study can be translated to a mechanical advantage consistent with the findings of P. Sahoo *et al*. The work by C.S. Kumar *et al.* (2020), which examined TiAlCrN coatings through FEM integrated with experimental validation, highlighted the importance of coating layers in reducing friction, modifying chip formation, and restricting temperature rise. This aligns with the present study's demonstration that multilayer systems incorporating ceramic layers outperform single layer coatings in limiting heat diffusion. However, unlike C.S. Kumar *et al.*, who reported coating dependent changes in chip morphology (such as secondary serrated teeth), the current study did not specifically address chip formation mechanisms. Instead, it provides new insight into the temperature evolution around the secondary shear zone, offering complementary thermal evidence that may explain the coating dependent chip behaviour observed in previous research.

Previous thermal analyses of coated cutting tools by R.F. Brito *et al.* (2009) have shown that ceramic coatings significantly influence temperature distribution within the tool by restricting heat transfer toward the substrate. These findings are consistent with the present results, where the TiN/Al_2O_3 multilayer configuration exhibited reduced internal temperatures and lower thermal gradients compared with single-layer coatings. The thermal behaviour observed in the present study was closely related to the fundamental mechanisms governing heat generation during cutting. Classical cutting theory, as described by P. Albrecht (1960), emphasised the contribution of ploughing and frictional interactions at the tool-chip interface, which became dominant under conditions of high contact pressure and limited lubrication. These mechanisms directly explained the rapid temperature rise and pronounced thermal gradients observed in the uncoated WC-Co insert, where no thermal barrier was present to restrict heat penetration. The transient nature of temperature evolution obtained in this work was consistent with the findings of P.A.R. Rosa *et al.* (2007), who demonstrated that the initial phase of machining was characterised by a rapid increase in thermal and mechanical loads before reaching a quasi-steady state. In the present results, all tool configurations reached their maximum surface temperature at approximately 6 ms, confirming that the early transient regime played a critical role in defining the overall thermal response of coated and uncoated tools. The differences observed between single-layer and multilayer coatings during this transient phase further highlighted the influence of coating architecture on heat accumulation near the cutting edge. Although S.M. Afazov *et al.* (2010) primarily focused on force prediction in micro-milling, their numerical framework underscored the strong coupling between mechanical loading, frictional behaviour, and thermal effects in cutting processes. The present FEM results extended this perspective by demonstrating that coating architecture not only affected mechanical interaction but also governed the redistribution of heat within the tool. In particular, the reduced internal temperatures observed for the TiN/Al_2O_3 multilayer configuration indicated that ceramic layers effectively decoupled surface heat generation from substrate thermal loading, thereby mitigating internal thermal gradients. Overall, the agreement between classical cutting theory, transient machining analyses, and the present FEM-based thermal results supported the conclusion that accurate thermal modelling had to account for both transient effects and coating architecture. The present study reinforced the necessity of experimentally validated numerical models to capture these coupled phenomena and to guide the design of advanced coating systems for dry machining applications.

A key contribution of the present study lies in its detailed evaluation of temperature evolution near, though not directly at, the tool rake face, which experimental tools often fail to capture accurately. The integration of experimentally validated FEM modelling therefore bridges a persistent measurement gap in machining research. The results notably highlight the superior thermal resistance of Al_2O_3, validating its role as an efficient thermal barrier layer. Conversely, they confirm the weak thermal protection provided by TiN, reinforcing long standing hypotheses with new quantitative data. Another essential contribution is the recognition of cutting condition variability as a significant limitation affecting the predictive accuracy of thermal models. This point has been insufficiently addressed in many analytical studies. The current research also confirms and extends findings from earlier studies by offering validated FEM-based insights into the heat transfer behaviour of coated cutting tools. Through a direct comparison of CVD layers and a double coated configuration, the study provides refined quantitative evidence of the thermal advantages of ceramic based coatings. It clarifies the limitations of metallic coatings, such as TiN. By emphasising temperature development near the secondary shear zone and addressing modelling uncertainties arising from cutting condition variability, this work deepens the understanding of coating performance in dry machining. It establishes a robust foundation for future investigations into thermally driven tool degradation, coating optimisation, and microstructural behaviour under high thermal loads.

CONCLUSIONS

In this study, FEM was employed through numerical and theoretical analysis to examine the performance of two distinct coating layers under dry orthogonal cutting conditions. The analysis considered two commercially available CVD coated tools and a double coated tool. The numerical approach, after having been validated by comparing to experimental data, provided valuable insights into the thermal field and its temporal changes in the vicinity of the secondary shear zone, which could complement experimental techniques aimed at measuring temperatures near, but not directly on, the tool rake face. The findings of the present study emphasise the high efficiency of the coating system in controlling heat transfer during dry machining, with all tool configurations reaching their maximum surface temperature at approximately t ≈ 6 ms. From the combined numerical and experimental analysis of the temperature evolution, it may be derived that the uncoated WC-Co insert exhibits rapid heat penetration, reaching a peak surface temperature of about 456°C. The TiN-coated system results in a smoother temperature evolution, attaining a maximum of approximately 480°C, although it provides only limited thermal resistance. For the same reason, the double-coated configuration exhibits a greater surface temperature peak, reaching about 544°C, as the TiN/Al_2O_3 multilayer effectively restricts heat diffusion toward the substrate. This further increases the impact of the multi- or double-coated insert, since the Al_2O_3 layer acts as a highly efficient thermal barrier by confining heat near the cutting edge and protecting the WC-Co core from excessive thermal loading.

Based on the outcomes, the results obtained in the present work clearly indicate that the role of coating architecture,particularly the incorporation of an Al_2O_3 layer, is decisive in governing heat transfer function and enhancing substrate protection. Future work will focus on extending the proposed FEM framework to investigate the effects of coating architecture, layer thickness, and cutting conditions on thermomechanical behaviour and tool performance in dry machining.

ACKNOWLEDGEMENTS

None.

FUNDING

None.

CONFLICT OF INTEREST

None.

REFERENCES

[1] Afazov, S.M., Ratchev, S.M., & Segal, J. (2010). Modelling and simulation of micro-milling cutting forces. *Journal of Materials Processing Technology*, 210(15), 2154-2162. doi: 10.1016/j.jmatprotec.2010.07.033.

[2] Ala, M., Liu, W., Liu, H., & Wang, F. (2025). Investigation of cladding track geometry using thermal finite element method in laser cladding additive manufacturing. *The International Journal of Advanced Manufacturing Technology*, 138, 4593-4614. doi: 10.1007/s00170-025-15804-4.

[3] Albrecht, P. (1960). New developments in the theory of the metal-cutting process: Part I. The ploughing process in metal cutting. *Journal of Engineering for Industry*, 82(4), 348-357. doi: 10.1115/1.3664242.

[4] Bencheikh, I., Bilteryst, F., & Nouari, M. (2017). Modelling of the thermomechanical behaviour of coated structures using single and multi-level-set techniques coupled with the eXtended Finite Element Method. *Finite Elements in Analysis and Design*, 134, 68-81. doi: 10.1016/j.finel.2017.06.001.

[5] Brito, R.F., de Carvalho, S.R., Marcondes de Lima e Silva, S.M., & Ferreira, J.R. (2009). Thermal analysis in coated cutting tools. *International Communications in Heat and Mass Transfer,* 36(4), 314-321. doi: 10.1016/j.icheatmasstransfer.2009.01.009.

[6] Grzesik, W., Bartoszuk, M., & Nieslony, P. (2005). Finite difference method-based simulation of temperature fields for application to orthogonal cutting with coated tools. *Machining Science and Technology*, 9(4), 529-546. doi: 10.1080/10910340500398258.

[7] Ifis, A., Bilteryst, F., & Nouari, M. (2013). Transient thermomechanical analysis of thin layers using a hybrid "MAX-FEM" model. *Finite Elements in Analysis and Design*, 69, 73-87. doi: 10.1016/j.finel.2013.01.008.

[8] Ipilakyaa, T.D., Tuleun, L.T., & Injor, O.M. (2024). Heat transfer modelling of multilayer coated tools during turning of H13 hardened steel: Analogous coating layer approach. *Saudi Journal of Engineering and Technology*, 9(4), 205-213. doi: 10.36348/sjet.2024.v09i04.002.

[9] Komanduri, R., & Hou, Z.B. (2001). Analysis of heat partition and temperature distribution in sliding systems. *Wear*, 251(1-12), 925-938. doi: 10.1016/S0043-1648(01)00707-4.

[10] Kone, F., Czarnota, C., Haddag, B., & Nouari, M. (2011). Finite element modelling of the thermo-mechanical behavior of coatings under extreme contact loading in dry machining. *Surface and Coatings Technology*, 205(12), 3559-3566. doi: 10.1016/j.surfcoat.2010.12.024.

[11] Kumar, C.S., Zeman, P., & Polcar, T. (2020). A 2D finite element approach for predicting the machining performance of nanolayered TiAlCrN coating on WC-Co cutting tool during dry turning of AISI 1045 steel. *Ceramics International*, 46(16), 25073-25088. doi: 10.1016/j.ceramint.2020.06.294.

[12] Kumaran, G., Sivaraj, R., Prasad, V.R., Beg, O.A., Leung, H.H., & Kamalov, F. (2021). Numerical study of axisymmetric magneto-gyrotactic bioconvection in non-Fourier tangent hyperbolic nano-functional reactive coating flow of a cylindrical body in porous media. *The European Physical Journal Plus*, 136(11), article number 1107. doi: 10.1140/epjp/s13360-021-02099-z.

[13] Lazoglu, I., & Altintas, Y. (2002). Prediction of tool and chip temperature in continuous and interrupted machining. *International Journal of Machine Tools and Manufacture*, 42(9), 1011-1022. doi: 10.1016/S0890-6955(02)00039-1.

[14] Nguyen, D.H., Bilteryst, F., Lazard, M., Lamesle, P., & Dour, G. (2008). Coupling of the eXtended Finite Element Method and the matching asymptotic development in the modelling of brazed assembly. I*nternational Journal*

of Material Forming, 1, 1119-1122. doi: 10.1007/s12289-008-0176-z.
[15] Rosa, P.A.R., Kolednik, O., Martins, P.A.F., & Atkins, A.G. (2007). The transient beginning to machining and the transition to steady-state cutting. *International Journal of Machine Tools and Manufacture*, 47(12-13), 1904-1915. doi: 10.1016/j.ijmachtools.2007.03.005.
[16] Sahoo, P., Patra, K., Singh, V.K., Gupta, M.K., Song, Q., Mia, M., & Pimenov, D.Y. (2020). Influences of TiAlN coating and limiting angles of flutes on prediction of cutting forces and dynamic stability in micro milling of die steel (P-20). *Journal of Materials Processing Technology*, 278, article number 116500. doi: 10.1016/j.jmatprotec.2019.116500.
[17] Schnaubelt, E., Wozniak, M., & Schöps, S. (2023). Thermal thin shell approximation towards finite element quench simulation. *Superconductor Science and Technology*, 36(4), article number 044004. doi: 10.1088/1361-6668/acbeea.
[18] Upadhyay, C., Rajput, S.S., Bera, S., Ju, H., Bhide, R., & Gangopadhyay, S. (2025). Influence of TiAlN coating thickness in dry machining of AISI 1045 steel using Finite Element simulation and experiments. *Surface and Coatings Technology*, 495, article number 131496. doi: 10.1016/j.surfcoat.2024.131496.
[19] Van Luttervelt, C.A., *et al.* (1998). Present situation and future trends in modelling of machining operations progress report of the CIRP Working Group 'Modelling of machining operations'. *CIRP Annals*, 47(2), 587-626. doi: 10.1016/S0007-8506(07)63244-2.
[20] Zhang, J., Zhang, G., & Fan, G. (2022). Effects of tool coating materials and coating thickness on cutting temperature distribution with coated tools. *International Journal of Applied Ceramic Technology*, 19(4), 2276-2284. doi: 10.1111/ijac.14038.

Абдельхак Сауді
Аспірант
Лабораторія інженерії та науки про перспективні матеріали (ISMA)
Кафедра машинобудування, Університет ABBES Лагрур
40004, а/с 1252, дорога Батна, м. Хеншела, Алжир
https://orcid.org/0000-0002-8295-1947

Белькассем Меддур
Професор
Лабораторія інженерії та науки про перспективні матеріали (ISMA)
Кафедра машинобудування, Університет ABBES Лагрур
40004, а/с 1252, дорога Батна, м. Хеншела, Алжир
https://orcid.org/0000-0002-4751-2615

Бадіс Хаддаг
Доцент
Лабораторія LEM3, UMR CNRS 7239, Університет Лотарингії
Інститут гірничої справи та телекомунікацій (InSIC)
88100, вул. Voie de l'Innovation, 27, м. Сен-Дьє, Франція
https://orcid.org/0000-0003-3850-3044

Мохаммед Салах Аггун
Доктор філософії з інженерії матеріалів
Факультет науки і технологій, кафедра машинобудування
Університет Ечахіда Шейха Ларбі Тебессі
12000, м. Тебесса, Алжир
https://orcid.org/0000-0002-3385-7081

Абдельазіз Аббуді
Професор
Лабораторія інженерії та науки про перспективні матеріали (ISMA)
Кафедра машинобудування, Університет ABBES Лагрур
40004, а/с 1252, дорога Батна, м. Хеншела, Алжир
https://orcid.org/0000-0002-1398-6070

Моделювання та дослідження теплової поведінки тонкого шару методом скінченних елементів – застосування до інструментів з покриттями

Анотація. Безперервний розвиток технологій тонких шарів є ключовим для сучасного сухого оброблення, де ефективний тепловий контроль різальних інструментів з покриттями має вирішальне значення для обмеження теплово зумовленого зносу та подовження терміну служби інструмента. Метою цієї статті було дослідження та моделювання теплової реакції різальних інструментів з покриттями, а також оцінка впливу одношарових і багатошарових тонких покриттів на теплоперенос під час ортогонального сухого різання. Для досягнення цієї мети була розроблена нестаціонарна теплова модель на основі методу скінченних елементів із використанням формулювання Галеркіна в поєднанні з неявною часовою схемою Кранка-Ніколсона. Чисельний підхід було застосовано до трьох конфігурацій інструмента: різальної пластини без покриття з WC-Co, пластини з покриттям TiN та пластини з двошаровим покриттям TiN/Al_2O_3. Для валідації чисельних прогнозів були проведені експериментальні випробування сухого точіння. Отримані результати показали, що чисельна модель точно відтворює часову еволюцію температури на межі інструмент–стружка та всередині різальної пластини. Інструмент без покриття характеризується швидким проникненням тепла та вираженими внутрішніми тепловими градієнтами. Покриття TiN дещо підвищує температуру поверхні, проте забезпечує обмежений опір тепловій дифузії. Натомість багатошарова конфігурація TiN/Al_2O_3 суттєво обмежує теплоперенос у напрямку підкладки, що призводить до нижчих внутрішніх температур і зменшення теплових градієнтів. Шар Al_2O_3 діє як ефективний тепловий бар'єр, локалізуючи тепло поблизу різальної кромки та захищаючи серцевину інструмента від надмірного теплового навантаження. Отримані результати свідчать, що багатошарові керамічні покриття забезпечують кращий тепловий захист порівняно з одношаровими. Запропонований підхід на основі методу скінченних елементів може бути ефективно застосований для проєктування покриттів, оптимізації інструментів і керування тепловими процесами в умовах сухого оброблення

Ключові слова: сухе оброблення; теплоперенос; чисельний підхід; різання; нестаціонарність